Remote Drone Detection and Localization with Fiber-Optic Microphones and Distributed Acoustic Sensing

Jian Fang, Yaowen Li, Philip N. Ji, and Ting Wang
NEC Laboratories America Inc., Princeton, NJ 08540, USA.
jfang@nec-labs.com

Abstract: We demonstrate the first fiber-optic drone detection method with ultra-highly sensitive optical microphones and distributed acoustic sensor. Accurate drone localization has been achieved through acoustic field mapping and data fusion. © 2022 The Author(s)

1. Introduction

The class I unmanned aerial vehicles (UAVs), which are also known as drones, have become increasingly prevalent in a variety of applications, including battling forest fires, assisting search/rescue operations, and protecting homeland security. Unauthorized drones, on the other hand, have been reported as a nuisance on the airport runways, as well as being used as drug couriers, or spying on unsuspecting bystanders. Therefore, the detection and localization of unauthorized drones have been essentially desirable for both safety and security purposes. Conventional drone detection techniques include using Radar, LiDAR, camera, and acoustic sensors [1]. Among them, acoustics drone detection has advantages of capability under the non-line-of-sight environment and computation-effective on resource requirements [2]. Electrical microphones are commonly used in conventional acoustic drone detection. However, in the practical sense, it is very difficult for electrical microphones to serve large-scale applications, such as airport protection or city-wise monitoring. The numerous microphones have a heavy bundle of metal wires, raising the cost of installation and handling. The synchronization of these microphones is also challenging and requires additional devices. Electro-magnetic interference (EMI) shielding is essential for reliable measurement. The acquisition and transfer of acoustic data need many recorders and switches that drastically increase the cost and complexity.

In this work, we present the first fiber-optic approach to detect and localize the drone remotely. Instead of using the electrical microphones array in conventional methods, we utilize the ultra-highly sensitive fiber-optic microphones (FOMs) to detect the drone signal. Compared with electrical microphones, the fiber-optics microphones are fully passive, EMI-immune, and optically synchronized, giving the advantages of cost-effective coverage for large-scale applications. With the help of fiber-optic distributed acoustic sensing technology, the acoustic field can be mapped in 3D space, allowing for accurate angle localization. The acoustic field can further combine with visual data through data fusion, providing an augmented view of reality to better understand the events.

2. Ultra-Highly Sensitive Fiber-Optic Microphone

Fiber-optic distributed acoustic sensing (DAS) technology has been applied to a wide range of applications such as seismic activity detection [3], traffic monitoring [4], and pipeline protection [5], for its intriguing feature of detecting the vibration along the buried fiber over a long distance. On the other hand, detecting the acoustics in the air has been

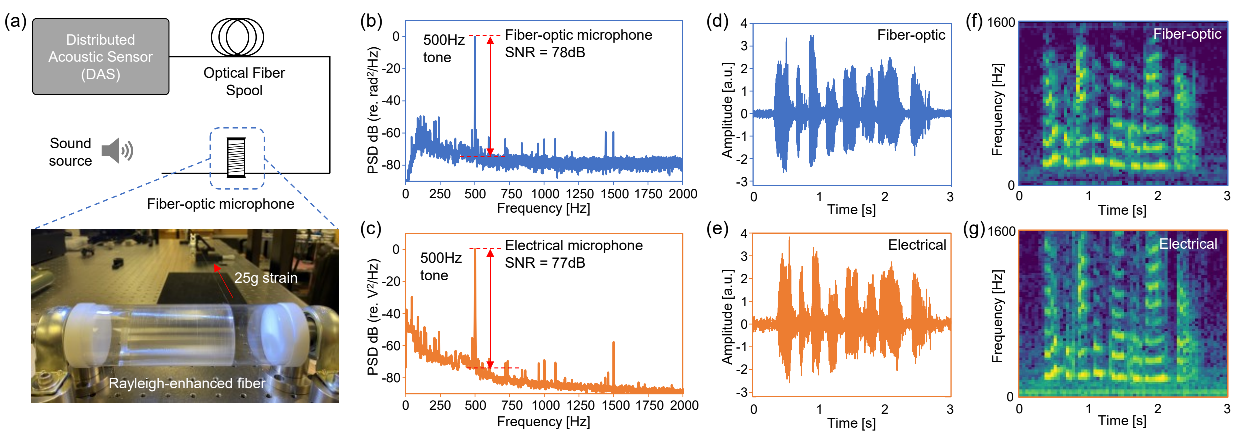

Fig. 1. (a) Test setup (upper) and manufacturing process (lower) of the fiber-optic microphone. (b) and (c) are the normalized spectra of a 500Hz tone recorded by fiber-optic microphone (b) and electrical microphone (c), respectively. (d) and (e) are the speech waveforms from Harvard Sentences recorded by the fiber-optic (d) and electrical (e) microphones. (f) and (g) are the corresponding spectrograms of (d) and (e), respectively.

a very challenging task for DAS due to two main limitations: (1) the regular single-mode fiber is relatively insensitive to normal sound pressure; (2) the DAS sensitivity decreases with the fiber distance [6]. To overcome both limitations, we develop ultra-highly sensitive fiber-optic microphones (FOMs), which employ the Rayleigh-enhanced optical fiber [7] and ultra-thin-wall cylinders. As shown in Fig. 1(a), the FOMs were manufactured by applying 25-gram strain on the Rayleigh-enhanced fiber, and then densely wrapping 60-m of the fiber on the outer surface of the cylinder. The Rayleigh-enhanced fiber was prepared through UV processing, creating quasi-continuous incoherent scatterers which boost the in-band Rayleigh scattering power. The ultra-thin wall cylinders are made of glycol-modified polyethylene terephthalate (PETG) with Young's modulus of 2.1GPa and Poisson's ratio of 0.34. The length, diameter, and thickness of the cylinder are 120.0mm, 50.8mm, and 0.46mm, respectively. The theoretical sensitivity of our FOM is −96.70dB re.1rad/μPa, calculated with the equations in [8]. To verify that, a DAS system was connected to the FOM through an optical fiber spool, while a speaker was placed 0.5 m away from the FOM. The speaker generated a 500Hz tone with a sound pressure level (SPL) of 78.5dB (measured near the FOM). A modern back-electret condenser microphone with ultra-flat response was placed next to the FOM as the reference. Fig. 1(b) and (c) demonstrate the normalized spectra of the 500Hz tone. Note that the DAS has a build-in high-pass filter (HPF) so that the frequency components near DC were minimized. Signals from DC to 240Hz are due to the background noise in the test environment. It can be found that the SNR of FOM is around 78dB, which is slightly better than the electrical microphone. Moreover, the spectrum of FOM appears flatter than the electrical one. The phase change $\Delta\varphi$ of FOM is 1.60rad. Considering the SPL of 78.5dB, the measured sensitivity is −100.43dB re.1rad/μPa, which is 3.73dB lower than the theoretical prediction. The discrepancy may be from the effect of fiber layer and epoxy which are not considered in the theoretical model. Compared with the sensitivities of other FOMs in the literature (e.g., −136.9dB [9], −133.7dB [8], −130.1dB [10], −128dB [11] and −112dB [12], in the unit of re.1rad/μPa), our design has over 11.5dB improvement, allowing us to obtain more insights of the sound in the air.

We also tested the FOM performance on human speech detection by using the dataset of IEEE-Harvard Sentences List 1. Fig. 1 (d) and (e) illustrate the speech waveforms recorded by our FOM and the reference microphone, while Fig. 1(f) and (g) are their corresponding spectrograms, respectively. The pitches and breaks of tones are clearly evident on both spectrograms. The shape of waveforms is almost identical, while FOM has a smaller noise term due to the HPF in DAS. The insertion loss is only 0.2dB including two FC/APC connectors. The excellent agreement and comparable quality confirm that our FOM can be used in sound sensing applications, especially where the conventional electrical microphones are not practical.

3. Demonstration of Remote Drone Detection and Localization

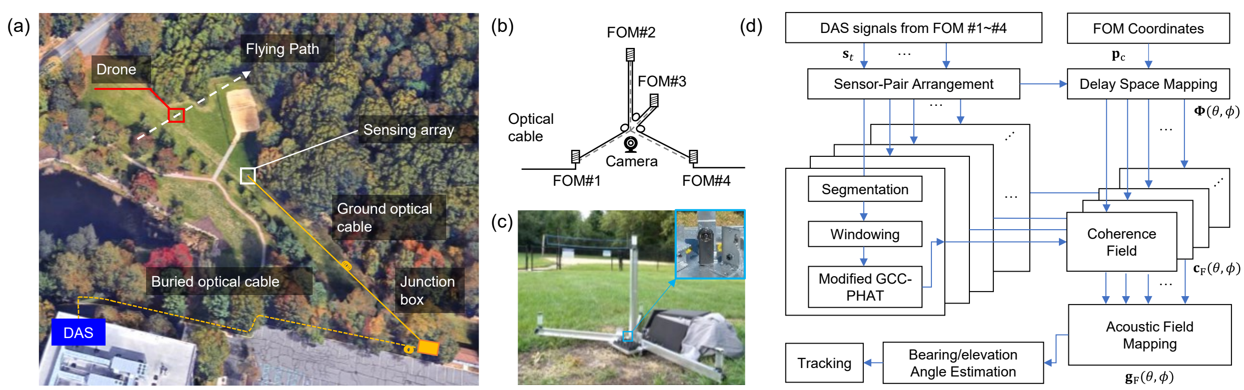

Fig. 2 (a) Setup for the outdoor drone detection experiment using DAS. (b) Structure of the fiber-optic sensing array. FOM: fiber-optic microphone. (c) Picture of the deployed fiber-optic sensing array with camera. (d) The steps of acoustic signal processing.

To demonstrate the capability of remote drone detection, we conducted field experiments as configured in Fig. 2(a). The DAS system in the building was connected to the fiber-optic sensing array through 1-km buried and ground optical cables. The array had a tetrahedral structure, where four ultra-highly sensitive FOMs were attached to the arms of the array frames, as shown in Fig. 2(b). The length of each arm of the frame is about 1 meter. The array was deployed on the lawn with a camera placed in the center, as depicted in Fig. 2(c). A drone (Matrice 600) flew linearly above the lawn. To match the fiber length of our FOMs, the DAS gauge length was set to 60m at the FOM locations. The laser pulse repetition rate was 20kHz. Fig. 2(c) illustrates the steps of acoustic signal processing. The 4 channels of DAS signals $\mathbf{s}_t = [s_1(t), \cdots, s_4(t)]$ from FOMs were arranged into 6 sensor pairs. For each sensor pair, the time-domain signals were truncated into segments with a windowing function. The time difference of arrival was estimated by the modified generalized cross-correlation with phase transform (GCC-PHAT). In this work, the position of the sound source is defined as its bearing and elevation angles w.r.t. the ground center of the array. The relationship between the target angles and the channel delays was linked by mapping the angles into a delayed space $\mathbf{\Phi}(\theta,\phi)$, in which each element is the theoretical delay of a sensor pair. The delay space was then converted into the coherence field $\mathbf{c}_{\mathrm{F}}(\theta,\phi)$ by replacing the delay values with its indexed cross-correlation vector. The same process has been repeated for each sensor pair. The coherence fields of each pair were combined as the acoustic field mapping $\mathbf{g}_{\mathrm{F}}(\theta,\phi)$, which shows the plausibility of the acoustic source. Finally, the place of the sound source was estimated by selecting the angles with maximal acoustic field intensity.

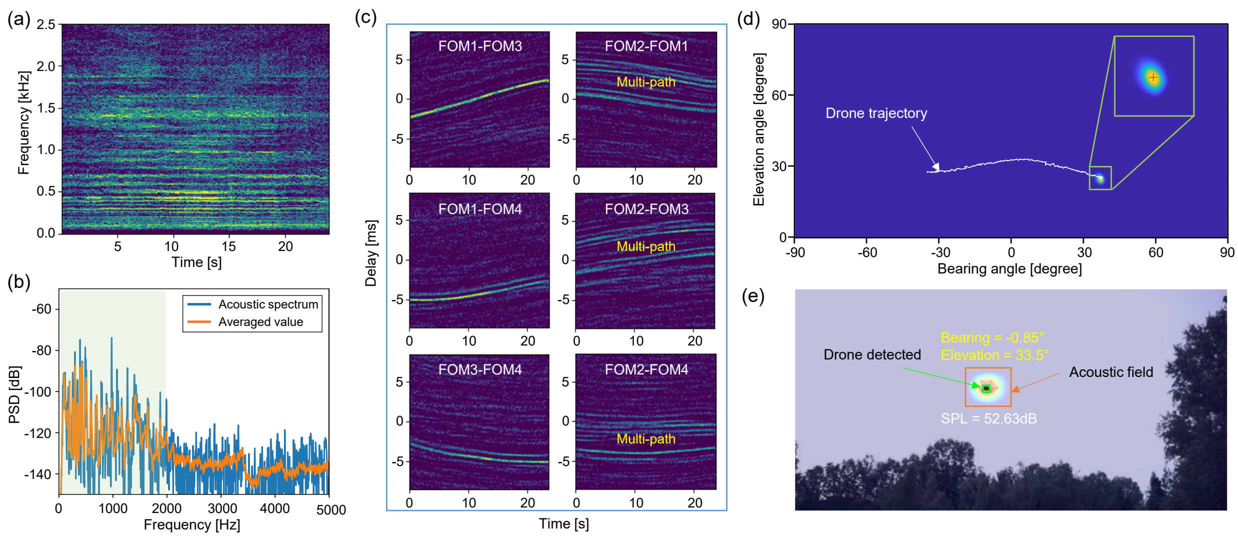

Fig. 3 (a) Spectrogram of the drone signal. (b) Detailed spectrum and averaged values. (c). Correlograms of all the sensor pairs. (d). Acoustic field and the tracked drone trajectory. (e). Augmented view from the data fusion between the global acoustic field and the camera's data.

The results of drone detection can be found in Fig. 3. Fig. 3(a) shows the spectrogram of the drone signal in 24 seconds recording, while Fig. 3(b) is the detailed spectrum and its averaged values. The acoustic signal was mainly from the rotation of blades, creating a harmonic-like pattern on the spectrogram. Most spectral components are below 2.5kHz, while the strongest harmonics are located within 20~500Hz. Fig. 3(c) illustrates the correlograms of all the sensor pairs. The distinct line in the left three correlograms implies a strong cross-correlation among the three ground FOMs, while the multiple lines in the right three indicate the multi-path effect from the ground reflection of the sound. After acoustic signal processing, the global acoustic field of the 3D space is mapped as Fig. 3(d), in which the sound of the drone was visualized as an acoustic pattern highlighted in the green boundary box. The drone's position was therefore determined at the maxima of the pattern (marked as red crossing) and tracked as the white curve in Fig. 3(d). The angle estimation accuracy (σ) is 0.266 degrees. In addition, we overlayed the global acoustic field with the camera's frames through data fusion, creating an augmented view of reality as Fig. 3(e). The data fusion result gives a multi-dimensional perception of the surrounding, including visual data, acoustic field, SPL from beamforming, and sound source location, which could be beneficial to better understand the surrounding environment.

4. Conclusion

We have, for the first time to our knowledge, demonstrated remote drone detection and localization using fiber-optic technology. By utilizing the Rayleigh-enhanced optical fiber and the ultra-thin-wall cylinders, we have achieved ultra-highly sensitive fiber-optic microphones with a measured sensitivity of -100.43dB re.1rad/μPa. The superior sensitivity implies the feasibility of detecting acoustics in the air with a DAS system even kilometers away. Results from field experiments have verified the effectiveness and accuracy of the proposed approach.

References

1. I. Guvenc, F. Koohifar, S. Singh, M. L. Sichitiu, and D. Matolak, IEEE Commun. Mag. **56**(4), 75–81 (2018).
2. Z. Shi, X. Chang, C. Yang, Z. Wu, and J. Wu, IEEE Trans. Veh. Technol. **69**(3), 2731–2739 (2020).
3. N. J. Lindsey, T. Craig Dawe, and J. B. Ajo-Franklin, Science **366**(6469), 1103–1107 (2019).
4. G. A. Wellbrock et al., in OFC (2019) Th3C.7.
5. J. Tejedor et al., J. Light. Technol. **34**(19), 4445–4453 (2016).
6. H. Gabai and A. Eyal, Opt. Lett. **41**(24), 5648 (2016).
7. P. S. Westbrook et al., iScience **23**(6), 101137 (2020).
8. M. J. Murray et al., J. Light. Technol. **36**(16), 3205-3210 (2018).
9. L. Ma et al., in AOPC (2019), 11340.
10. C. Li, Z. Mei, J. Tang, K. Yang, and M. Yang, in OFS (2018), Part F124.
11. L. Liu et al., IEEE Sens. J. **16**(9), 3054–3058 (2016).
12. H. Li et al., J. Light. Technol. **38**(4), 929–938 (2020).